Impact of Nonlinear Power Amplifier on BER Performance of OTFS Modulation

Sanjeev Sharma, Amit Singh, Kuntal Deka, Cédric Adjih

Impact of Nonlinear Power Amplifier on BER Performance of OTFS Modulation

Sanjeev Sharma[1], Amit Singh[1], Kuntal Deka[2], and Cedric Adjih[3]
[1]IIT (BHU) Varanasi, India [2]IIT Guwahati, India, and [3]INRIA, France
Email: {sanjeev.ece, amitsingh.rs.ece22}@iitbhu.ac.in, kuntaldeka@iitg.ac.in, cedric.adjih@inria.fr

***Abstract*—Recently, two dimensional orthogonal time frequency space (OTFS) modulation technique has introduced in wireless communications to combat the effects of multipath fading and Doppler spread. In this paper, we analyze the impact of nonlinear power amplifier (NPA) and phase noise on the OTFS system over the EVA channel model. The study focuses on the bit error rate (BER) performance concerning the input-back-off (IBO) and the nonlinearity parameter values of the NPA. The results demonstrate that both NPA and phase noise significantly degrade the OTFS system performance, especially for higher modulation schemes and low values of IBO. Furthermore, we numerically analyze the impact of system parameter variations on BER performance.**

***Index Terms*—Nonlinear Power Amplifier, OTFS, Phase Noise, BER Performance**

I. Introduction

Orthogonal Time Frequency and Space (OTFS) is an active area of research, and its potential applications include next-generation wireless communication systems, such as 5G and beyond, as well as emerging technologies like Internet of Things (IoT), unmanned aerial vehicles (UAVs), and vehicular communication [1]. OTFS is a modulation scheme that aims to overcome the limitations of traditional modulation techniques in challenging wireless communication environments such as doubly dispersive channel [2]. It was introduced as a new two-dimensional (2D) modulation scheme that leverages the delay-Doppler (DD) domain for robust communication in highly dispersive channels. OTFS is designed to combat the effects of delay spread, Doppler spread, and multipath fading, which can degrade the performance of communication systems. It achieves this by exploiting the sparsity of the channel in the DD domain, which is more resilient to these effects compared to the traditional time-frequency domain [3].

Researchers continue to explore various aspects of OTFS, including channel estimation, synchronization, equalization techniques, multiple-antenna systems, and the integration of OTFS with other advanced technologies. The goal is to further enhance its performance, address practical challenges, and explore its potential in various communication scenarios.

A. Motivations

Nonlinear power amplifier (NPA) in OTFS system introduces distortion and intermodulation products. OTFS relies on the orthogonality of DD grid to achieve high spectral efficiency, but the nonlinearity of the power amplifier can cause intermodulation distortion [4], resulting in interference between DD grids. This distortion can lead to increased in-band and out-of-band emissions and degradation of the OTFS system performance. Further, NPA can result in the inter-symbol interference (ISI) and inter-carrier interference (ICI) due to phase and amplitude distortion, degrading the overall system performance and reducing the achievable data rates and increased bit error rates (BER) [5]. To mitigate these issues, linearization techniques such as digital predistortion (DPD) can be employed to compensate for the nonlinear characteristics of the power amplifier. However, these techniques can add complexity and cost to the system implementation.

Further, phase noise (PN) refers to the random fluctuations in the phase of a signal over time. It is caused by various factors, such as imperfections in the local oscillators or frequency synthesizers used in the transmitter and receiver. These fluctuations can introduce errors in the demodulation process and degrade the performance of the OTFS system. PN can be mitigated by inserting known pilot symbols within the OTFS frame allows the receiver to estimate the PN and compensate for it during demodulation. Furtehr, adaptive algorithms can continuously track and adjust the receiver's local oscillator to maintain accurate carrier frequency and phase synchronization in OTFS system.

To analyze the performance of OTFS modulation in the presence of NPAs and PN can be an intriguing research direction. Thus, we consider impact of NPA and PN on OTFS's BER performance in this paper.

B. Related Prior Work

In [6], high peak to average power ratio (PAPR) of an OTFS system is analyzed. Due to the high PAPR of OTFS signals, they are prone to entering the nonlinear region of power amplifiers (PAs), leading to nonlinear distortion. In [7], nonlinear distortions in mmWave OTFS systems is considered. Channel estimation using pilot insertion method is analyzed in nonlinear scenario in OTFS [7]. Pilot power allocation problem is analyzed in [8]. Impact of PN is analyzed in [9, 10]. Impact of IQ (in-phase and quadrature-phase) imbalance in OTFS system is considered in [11]. Table I provides a summary of the analysis conducted for NPA and PN in OTFS. However, the joint impact of NPA and PN is not analyzed in OTFS literature for high mobility communication scenario. Therefore, by studying the joint impact of NPAs and PN in OTFS systems, we aim to gain insights into their combined effects, devise effective mitigation strategies, and ultimately

enhance the performance of OTFS in practical communication scenarios.

C. Contributions

In this paper, we investigate the performance of an OTFS system in the presence of NPAs and PN. We analyze the BER considering both the Extended Vehicular A model (EVA) [13] and Rayleigh fading channel models, incorporating various system parameters. Additionally, we explore the impact of different carrier frequencies and PN parameters on the system performance. Through these investigations, we highlight the need to develop techniques and algorithms that enhance the robustness and reliability of OTFS systems in real-world scenarios.

II. OTFS PRELIMINARIES

We provide a concise explanation of symbol representation in the DD domain signal modulation and demodulation process in the OTFS. In OTFS, the data symbols (like Quadrature Amplitude Modulation (QAM)) are organized on a 2D grid known as the DD plane, denoted as $\varphi_{N,M}$, where M and N represent the total number of delay and Doppler bins, respectively. The DD plane $\varphi_{N,M}$ accommodates a maximum of MN different QAM symbols. The transmitted input signal $x_{\mathrm{DD}}[k,l]$ corresponds to the symbol located at the intersection of the kth Doppler bin and the lth delay bin, where k ranges from 0 to $N-1$, and l ranges from 0 to $M-1$. Typically, the horizontal axis of $\varphi_{N,M}$ represents the M delay values, while the vertical axis represents the N Doppler shifts.

Suppose we have a data transmission frame with a duration of $T_{\mathrm{f}} = NT$ and a bandwidth of $B = M\triangle f$, where $\triangle f$ represents the sub-carrier frequency and T denotes the symbol duration. Here, T is determined by $T = \frac{1}{\triangle f}$. To ensure proper transmission, it is necessary to satisfy $\triangle f < \frac{1}{\tau_{\max}}$ and $\triangle\nu = \frac{1}{NT}$, where $\tau_{\max}$ represents the maximum delay spread and $\nu_{\max}$ corresponds to the maximum Doppler spread. The DD plane, $\varphi_{N,M}$, is characterized by a delay interval of $\triangle\tau = \frac{1}{M\triangle f}$ and a Doppler interval of $\triangle\nu = \frac{1}{NT}$. Therefore, to transmit MN symbols within a frame of duration T_f and bandwidth B, the selection of N and M is influenced by the delay and Doppler characteristics of the channel. A channel with a higher Doppler spread $\nu_{\max}$ would require a larger $N\triangle\nu$ leading to a smaller T and a larger $\triangle f$ thus necessitating a larger N and a smaller M. Similarly, a channel with a higher delay spread $\tau_{\max}$ would require a larger $M\triangle\tau$ leading to the selection of $\varphi_{N,M}$ with a larger M and a smaller N [13].

Basic Concept of OTFS Modulation-Demodulation: The OTFS system in the presence of NPA and PN is shown in Fig. 1, which uses modulation at the Tx and demodulation at the Rx. OTFS in the first stage operates in the DD domain, while the second stage after transform operates in the time-frequency domain.

To begin, the QAM symbols ($x_{\mathrm{DD}}[k,l]$s) intended for transmission are organized on the DD domain, represented by $\varphi_{N,M}$. These symbols are then transformed from the DD domain to the time-frequency domain using the inverse symplectic finite Fourier transform (ISFFT) as follows:

$$X_{\mathrm{TF}}[n,m] = \frac{1}{MN}\sum_{k=0}^{N-1}\sum_{l=0}^{M-1} x_{\mathrm{DD}}[k,l]e^{j2\pi(\frac{nk}{N}-\frac{ml}{M})}. \quad (1)$$

Similarly, at the receiver, the time-frequency domain received signals are ultimately converted back to the DD domain using the symplectic finite Fourier transform (SFFT) as follows:

$$y_{\mathrm{DD}}[k,l] = \sum_{n=0}^{N-1}\sum_{m=0}^{M-1} Y_{\mathrm{TF}}[n,m]e^{-j2\pi(\frac{nk}{N}-\frac{ml}{M})}. \quad (2)$$

Both the SFFT and the ISFFT can be understood as combining M-point inverse fast Fourier transforms (IFFTs) along each Doppler axis and N-point fast Fourier transforms (FFTs) along each delay axis, respectively. To ensure compatibility, the 2D grid must be confined to a dimension of $N \times M$. Therefore, a rectangular windowing function is employed at both the transmitter and the receiver to facilitate this limitation.

OTFS Operations in Time-frequency Domain : The Heisenberg transform is applied to convert a 2D modulated time-frequency domain signal into the time domain using a given basis pulse shape, $g_{\mathrm{tx}}(t)$, according to the following expression:

$$s(t) = \sum_{n=0}^{N-1}\sum_{m=0}^{M-1} X_{\mathrm{TF}}[n,m]e^{j2\pi m\triangle f(t-nT)}g_{\mathrm{tx}}(t-nT). \quad (3)$$

In the case of a rectangular pulse, equation (3) can be simplified to a series of M-point IFFTs along each time axis, leading to the generation of data in delay-time domain followed by a parallel-to-serial converter. Therefore, when $N = 1$, equation (3) corresponds to OFDM modulation. The transmitted signal, $s(t)$, is transmitted through the wireless channel with an impulse response denoted as $h_{\mathrm{DD}}(\tau,\nu)$. The signal $r(t)$ at receiver is expressed as follows:

$$r(t) = \iint h(\tau,\nu)e^{j2\pi\nu(t-\tau)}s(t-\tau)\,d\tau d\nu + z(t) \quad (4)$$

The received signal, $r(t)$, in the time domain, is affected by additive white Gaussian noise (AWGN), represented by $z(t)$. To convert the received signal, $r(t)$, into the time-frequency domain, the Wigner transform is applied, resulting in the representation $Y_{\mathrm{TF}}[n,m]$, where n and m denote the respective indices in the time-frequency domain as:

$$Y_{\mathrm{TF}}[n,m] = \int_{-\infty}^{\infty} g^{*}_{\mathrm{rx}}(t_1-nT)r(t)e^{-j2\pi m\Delta f(t_1-nT)}dt_1 \quad (5)$$

In equation (5), $g_{\mathrm{rx}}(t)$ represents the pulse used at the receiver. The rectangular pulse $g_{\mathrm{rx}}(t)$ in (5) simplifies to a series of M-point FFTs along each time axis after a serial-to-parallel conversion of the received signal $r(t)$. If $N = 1$ in (5), then correspondinf system represents an OFDM demodulation. It is crucial to carefully select $g_{\mathrm{tx}}(t)$ and $g_{\mathrm{rx}}(t)$ so that they ideally adhere to the bi-orthogonality property. Failure to satisfy this property can result in interference in the desired DD grid

TABLE I: A Summary of Representative Works on NPA and PN in OTFS

Reference	Work	Contribution
[6]	BER and PAPR analysis	OTFS system
[7]	BER analysis	nonlinear distortions are considered for OTFS
[8]	BER and PAPR analysis	Impact of pilot insertion in OTFS
[9, 10]	BER analysis	Phase noise in OTFS
[12]	BER analysis	LDPC Coded OTFS
[11]	BER analysis	IQ imbalance effect in OTFS
Proposed work	BER analysis	Impact of NPA and PN in OTFS

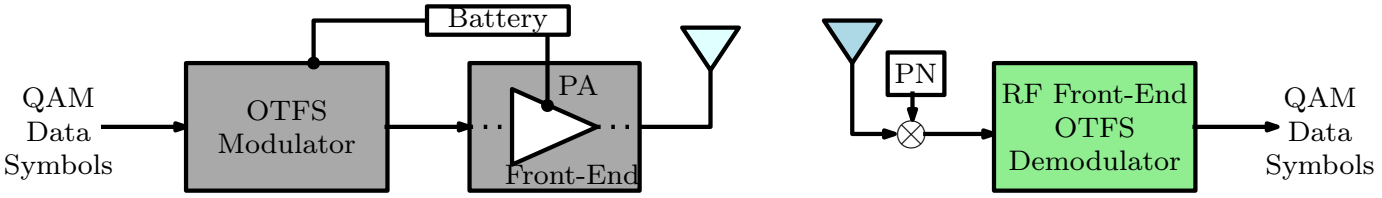

Fig. 1: Block diagram of OTFS system in the presence of NPA and phase noise (PN)

point from adjacent delay and Doppler bins. Further, the bi-orthogonality attribute of OTFS signals can be given as

$$\int e^{-j2\pi m\triangle f(t_1-nT)} g^*_{\text{rx}}(t_1 - nT) g_{\text{tx}}(t_1)\, dt_1 = \delta(m)\delta(n). \tag{6}$$

The pulses $g_{\text{tx}}(t)$ and $g_{\text{rx}}(t)$ that fulfill the bi-orthogonality property are referred to as ideal pulses. In the case of simple rectangular pulses, $g_{\text{tx}}(t)$ and $g_{\text{rx}}(t)$ have an amplitude of $1/\sqrt{T}$ for $t \in [0, T]$, and they are zero for all other values. While rectangular pulses do not strictly meet the bi-orthogonality condition, they are commonly used in simulations and analysis.

OTFS Input-Output Relation: The input-output relationship denotes to the relation between the $x_{\text{DD}}[k,l]$ values and the corresponding $u[k,l]$ values. This relationship plays a crucial role in developing detectors on the receiver side for OTFS system. The representation of the channel response $h_{\text{DD}}(\tau,\nu)$ in the DD domain can be effectively expressed as

$$h_{\text{DD}}(\tau,\nu) = \sum_{i=1}^{P_1} g_i \delta(\tau - \tau_i)\delta(\nu - \nu_i) \tag{7}$$

In the above equation, P_1 represents the count of paths present in the channel, and $\delta(.)$ symbolizes the Dirac delta function. The variables g_i, τ_i, and ν_i refer to the gain, delay, and Doppler shift of the ith path, respectively. Assuming independent and identically distributed channel coefficients and a uniform scattering profile, the gain h_i follows a complex normal distribution $h_i \sim \mathcal{CN}(0, \frac{1}{P})$. The delay and Doppler taps for the ith path is alternatively rewritten as follows:

$$\tau_i = \frac{l_{\tau_i}}{B}, \quad \nu_i = \frac{k_{\nu_i} + \kappa_{\nu_i}}{NT}, \tag{8}$$

where $B = M\triangle f$ is the total bandwidth of the system. Here, Doppler tap, delay tap, and fractional Doppler shift of the channel are represented by integer values k_{ν_i}, l_{τ_i} and κ_{ν_i}, respectively. Fractional Doppler shift values lie within the range of $[-0.5,\ 0.5]$. They are determined based on the delay and Doppler resolution of $\frac{1}{B}$ and $\frac{1}{NT}$, respectively. However, in some cases, $\frac{1}{NT}$ does not provide sufficient Doppler resolution, leading to the fractional Doppler shifts. Exploiting the sparse channel of the OTFS system, the signal ($y_{\text{DD}}[k,l]$s) at the receiver in the DD domain is expressed in terms of the transmitted signal ($x_{\text{DD}}[k,l]$s) for rectangular pulses as

$$\mathbf{y} = \mathbf{H}\mathbf{x} + \mathbf{z} \tag{9}$$

In the above representation, we have vectorized representation of the input signal ($x_{\text{DD}}[k,l]$s), output signal ($y_{\text{DD}}[k,l]$s), and AWGN (z) represented as $\mathbf{x} \in \mathbb{A}^{MN\times 1}$, $\mathbf{y} \in \mathbb{C}^{MN\times 1}$, and $\mathbf{z} \in \mathbb{C}^{MN\times 1}$, respectively. The coefficient matrix $\mathbf{H} \in \mathbb{C}^{MN\times MN}$ is responsible for establishing the relationship between them. To find the effective $\mathbf{H}$ for any practical waveform is described in [14]. The linear relationship described in equation (9) holds true for both ideal and practical pulses, even if values of channel $\mathbf{H}$ can vary. The non-zero values of the channel matrix $\mathbf{H}$ can be calculated as $S = \sum_{i=1}^{P_1}(2\tilde{N}+1)$, where $\tilde{N}$ represents the number of neighboring Doppler points that interfere with the specific point on the grid $\varphi_{M,N}$. When there are no fractional Doppler shifts (i.e., $\tilde{N} = 0$), we have $S = P_1$, and H a highly sparse channel. Due to the sparsity of $\mathbf{H}$, detection can be performed using message passing algorithm (MPA) [15]. Additionally, considering the block-circulant property of the $\mathbf{H}$ matrix, other low-complexity linear equalization algorithms such as the minimum mean square error (MMSE) signal detector is used for signal detection [15–17].

III. System Model

We transmit MN QAM symbols over wireless channels, and the output of the OTFS modulator is denoted as $\mathbf{x} = [x_1, ..., x_{MN}]^T$. A cyclic prefix (CP) of length N_{cp} is appended to the time-domain vector $\mathbf{x}$. Subsequently, the

sequence $\{x\}_n$ is fed through a memoryless nonlinear block $f(x)$ (shown in Fig. 1), resulting in the output samples:

$$y_n = f(x_n), \quad n = 1, ..., MN + N_{\text{cp}} - 1 \tag{10}$$

Nonlinear distortions introduced by $f(x)$ can cause significant out-of-band (OOB) radiation due to spectral regrowth effects. To mitigate this, the OOB-filtering block can be optionally applied to partially or completely suppress the OOB emission. Subsequently, the signal y_n is transmitted through a multipath channel with an impulse response h_n, resulting in the representation of the received signal as:

$$r_n = y_n \star h_n + w_n, \tag{11}$$

where symbol $\star$ denotes cyclic convolution, which holds the same value as linear convolution within the functional segment of the OTFS block when cyclic prefixes are appropriately incorporated. The expression w_n signifies AWGN featuring a mean of zero and a variance of σ_w^2.

A. Nonlinear power amplifier (NPA)

This paper explores the analysis of transmitter with memory-less nonlinearity, also referred to as polar nonlinearities, which are characterized by AM/AM and AM/PM conversion characteristics. Under such assumption, the baseband signal distorted in a NPA can be expressed as [18, 19]:

$$f(x_n) = F_{\text{A}}[|x_n|]e^{j(\arg[x_n]+F_{\text{P}}[|x_n|])}, \tag{12}$$

where $F_{\text{A}}[\cdot]$ and $F_{\text{P}}[\cdot]$ are functions that cause amplitude distortions (AM/AM conversion) and phase distortions (AM/PM conversion), respectability. This nonlinearity for solid-state power amplifiers (SSPA) is well represented by Rapp's model as [18]:

$$F_{\text{A}}[\rho] = \rho \left[1 + \left(\frac{\rho}{A_{\text{sat}}}\right)^{v}\right]^{-\frac{1}{v}}, \quad F_{\text{P}}[\rho] = 0 \tag{13}$$

where A_{sat} is the output saturation voltage and v is the smoothness factor. In general v ranges from 2 to 4. These models have gained a lot of popularity because they represent the power amplifier nonlinearity with simple analytical expressions. In general, operating point of the NPA is defined using the input back-bff (IBO) and it is defined as the ratio of saturation power P_{sat} of the NPA and the mean power P_{avg} of the input signal, i.e.,

$$\text{IBO} = 10\log_{10}\left[\frac{P_{\text{sat}}}{P_{\text{avg}}}\right] \text{ dB} \tag{14}$$

B. Phase noise (PN)

Incorporating the local oscillator (LO) PN $\theta(t)$ in radians, the RF signal can be mathematically represented as follows:

$$z(t) = y(t)e^{[j2\pi f_c t + \theta(t)]} = y(t)e^{j2\pi f_c t}e^{j\theta(t)} \tag{15}$$

The PN $\theta(t)$ is typically characterized in the frequency domain through its power spectral density (PSD) in dBc/Hz (decibels relative to the carrier per Hertz). This metric represents the ratio between the noise power level measured within a 1 Hz bandwidth, at a frequency offset from the carrier frequency f_m, and the power of the carrier [20]. In Fig. 2, we can observe the representation of this trait, where perfect oscillators are symbolized by a Dirac function in the frequency domain. In contrast, actual oscillators showcase a "skirt" pattern attributed to the PN profile. Within a classical depiction of stationary PN $\theta(t)$, it is portrayed as a Gaussian process at rest, characterized by a mean of zero and a distinct power spectral density of $\sigma^2_{\theta(t)}$ [21]. Thus, the received signal in (9), in the prescience of NPA and PN is given as

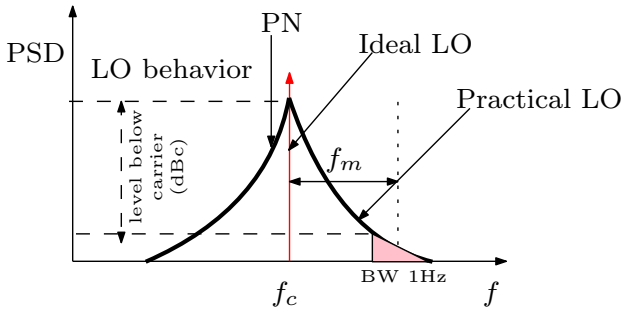

Fig. 2: Phase noise in local oscillator with ideal oscillator and practical oscillator. PN power level in dBc/Hz with f_m offset.

$$\mathbf{y} = \mathbf{H}\left[f(\mathbf{x})e^{j\boldsymbol{\theta}}\right] + \mathbf{z}, \tag{16}$$

where $\boldsymbol{\theta}$ is the discrete samples of the PN corresponding $\theta(t)$.

IV. Simulation Results and Discussion

We present the BER analysis of the OTFS system in the presence of NPA and PN. An MMSE detector [22] is used for data symbol detection. Furthermore, simulation parameters are given in Table II.

TABLE II: Simulation Parameters

S No.	Parameter	Values
1.	Carrier frequency f_c	2GHz
2.	Modulation	QPSK
3.	Doppler frequency shift	1KHz
4.	Pulse shaping	Ideal pulse
5.	Demodulation	MMSE
6.	Bandwidth	30 KHz
7.	M, N	4,8,16,,32,64
8.	Number of paths	2, 9 [EVA]
9.	Simulation tool	Matlab

Average BER performance of OTFS system in the presence of Rayleigh fading channel is shown in Fig. 3. Channel has two paths. For higher value of M and N, BER performance improves due to more channel diversity as observed in Fig. 3.

In Fig. 4, the average BER of the OTFS system in the presence of NPA is analyzed over the EVA channel model by considering different values of IBO and v. EVA channel parameters are mentioned in Table III. The results demonstrate that the BER performance is degraded when NPAs are present

TABLE III: Extended Vehicular A model (EVA) channel model parameters [22]

Path$_i$	1	2	3	4	5	6	7	8	9
Dealy τ_i (ns)	0	30	150	310	370	710	1090	1730	2510
Gain P_i (dB)	0	-1.5	-1.4	-3.6	-0.6	-9.1	-7	-12	-16.9

*Doppler of each path is generated using $f_{\max}\cos(\theta),\ \theta \in (0, 2\pi]$

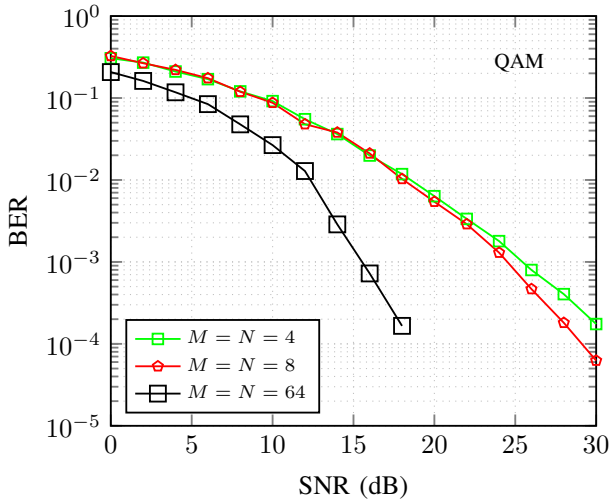

Fig. 3: BER vs SNR performance over Rayleigh channel. Doppler of each path is generated using $1000\cos(\theta)$Hz, where $\theta \in (-\pi, \pi]$. Two taps channel model is used with delay=[0, 1], Doppler=[0, 1] and uniform channel gain.

compared to the case without NPAs. As IBO increases, BER performance improves, as observed in Fig. 4. Additionally, it is observed that a smaller value of v leads to an increased BER in the OTFS system.

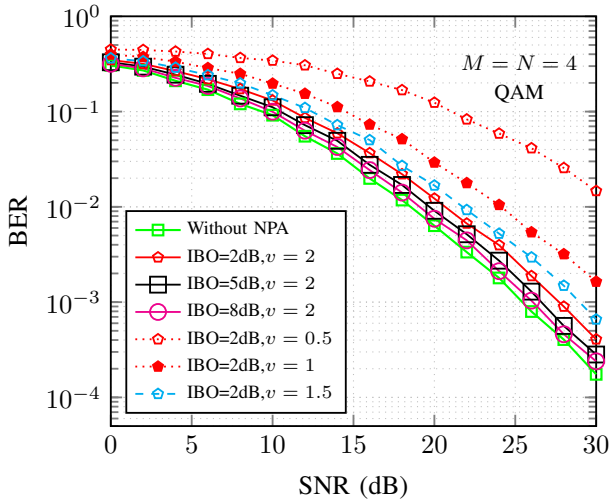

Fig. 4: Average BER vs SNR performance in the presence of NPA over EVA channel model.

Fig. 5 illustrates the impact of the DD grid parameters M and N in the presence of NPA. The results indicate that the BER performance is adversely affected when NPAs are present compared to the case without NPAs, regardless of the values of M and N. However, as the values of M and N increase, the BER performance shows improvement due to enhanced path diversity within the OTFS system. Furtehr, Fig. 6 demonstrates the impact of phase noise on the BER performance of the OTFS system. It reveals that higher phase noise power leads to a degradation in the BER performance. Moreover, the study observed that increasing the carrier frequency exacerbates the effect of PN, as evident from the trends observed in Fig. 6

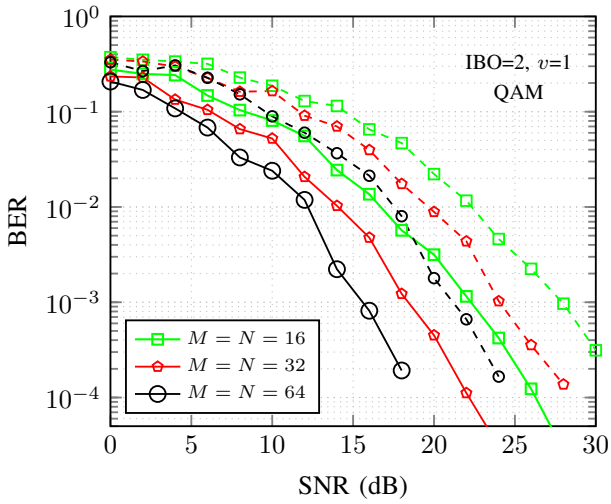

Fig. 5: BER vs SNR performance with and without NPA for different values of M and N over EVA channel. Solid and dashed lines denote the performance without and with NPA, respectively.

Next, we examine the impact of modulation order (QAM) in the presence of both NPA and PN, as depicted in Fig. 7 over the EVA channel. Notably, the performance of higher modulation schemes (e.g., QAM-16) experiences a significant deterioration when subjected to NPA, in contrast to the lower order modulations (e.g., QAM-2, QAM-4), as shown in Fig. 7. Furthermore, our results indicate that the influence of PN is comparatively lower when compared to the impact of NPA on the system's performance, as observed in the numerical outcomes in Fig. 7.

V. Conclusion

This paper has focused on investigating the impact of nonlinear power amplifiers (NPA) and phase noise (PN) on the OTFS system when operating over the EVA channel model. The study also examines the effects of NPA's parameters, such as input back-off (IBO) and smoothing parameters. The findings indicate that a lower value of IBO leads to higher distortion in the OTFS system. Additionally, the we explore

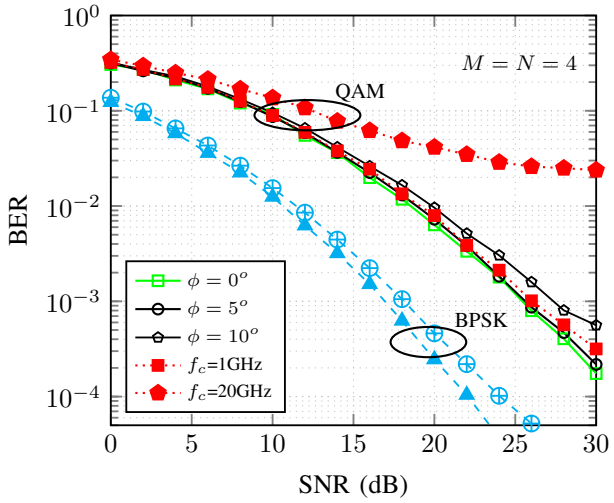

Fig. 6: BER vs SNR performance in the presence of phase noise using different PN power ϕ over EVA channel.

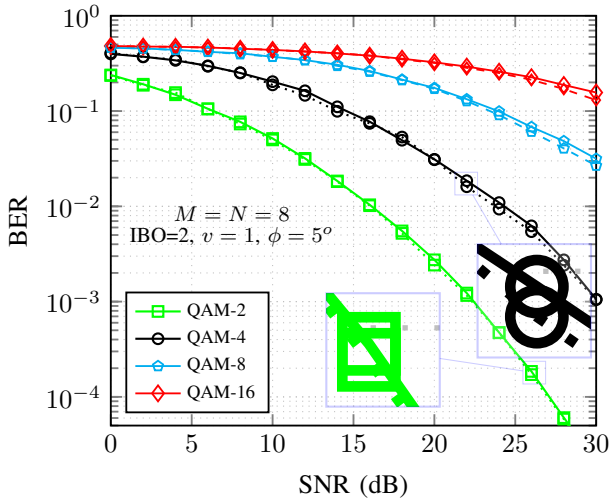

Fig. 7: BER vs SNR performance over EVA channel by varying modulation order. Dashed and solid lines represent the performance in the presence of NPA and PN plus NPA, respectively.

the influence of PN power and carrier frequency on the OTFS system. It also highlights the impact of OTFS parameters and modulation order in the presence of both NPA and PN on the system's BER performance.

The results demonstrate that NPA necessitates robust signal detection algorithms in the OTFS system to minimize its negative impact on BER performance. The study highlight the importance of addressing NPA-related challenges in order to optimize the performance of the OTFS system over the EVA channel model.

Acknowledgement

The authors would like to thank SERB, Govt. of India, IIT (BHU) Varanasi, MNNIT Allahabad, and University of Technology, Netherlands for all the support. This research is supported by Ministry of Science and Technology, SERB under Grant SRG/2021/000199-C and CRG/2023/005095.

References

[1] M. Qian, F. Ji, Y. Ge, M. Wen, X. Cheng, and H. V. Poor, "Block-wise index modulation and receiver design for high-mobility OTFS communications," *IEEE Trans. on Commun.*, 2023.

[2] Y. Chen, L. Zhao, Y. Jiang, W. Li, H. Gao, and C. Liu, "OTFS waveform based on 3-D signal constellation for time-variant channels," *IEEE Commun. Lett.*, vol. 27, no. 8, pp. 1999–2003, 2023.

[3] A. S. Bora, K. T. Phan, and Y. Hong, "IRS-assisted high mobility communications using OTFS modulation," *IEEE Wireless Commun. Lett.*, vol. 12, no. 2, pp. 376–380, 2022.

[4] J. Hou, J. Ge, D. Zhai, and J. Li, "Peak-to-average power ratio reduction of OFDM signals with nonlinear companding scheme," *IEEE Trans. on Broadcast.*, vol. 56, no. 2, pp. 258–262, 2010.

[5] O. B. H. Belkacem, R. Dinis, and M. L. Ammari, "Nonlinear effects in NOMA-OFDM systems: Analytical signal characterization and receiver design," *IEEE Trans. on Veh. Technol.*, vol. 72, no. 3, pp. 3739–3750, 2022.

[6] X. Xu, P. Yang, B. Zhang, Y. Xiao, and S. Li, "An improved PAPR reduction method based on imperialist competition algorithm for OTFS system," in *2022 IEEE 96th Veh. Technol. Conf. (VTC2022-Fall), London, United Kingdom*. IEEE, 2022, pp. 1–6.

[7] P. Priya, C. S. Reddy, and D. Sen, "Channel estimator and nonlinear detector for Mmwave beamformed OTFS systems in high mobility scenarios," *IEEE Trans. on Veh. Technol.*, vol. 72, no. 9, pp. 11 698–11 713, 2023.

[8] R. Marsalek, J. Blumenstein, A. Prokes, and T. Gotthans, "Orthogonal time frequency space modulation: Pilot power allocation and nonlinear power amplifiers," in *2019 IEEE Int. Symp. on Signal Process. and Inf. Technol. (ISSPIT), Ajman, United Arab Emirates*. IEEE, 2019, pp. 1–4.

[9] G. Surabhi, M. K. Ramachandran, and A. Chockalingam, "OTFS modulation with phase noise in mmWave communications," in *2019 IEEE 89th Veh. Technol. Conf. (VTC2019-Spring), Kuala Lumpur, Malaysia*. IEEE, 2019, pp. 1–5.

[10] Y. Bello, S. Barnola, D. Demmer, and J.-B. Doré, "OTFS waveform with phase noise in sub-THz," in *2022 IEEE 96th Veh. Technol. Conf. (VTC2022-Fall), London, United Kingdom*. IEEE, 2022, pp. 1–5.

[11] S. G. Neelam and P. Sahu, "Digital compensation of IQ imbalance, DC offset for zero-padded OTFS systems," *IEEE Commun. Lett.*, vol. 26, no. 10, pp. 2450–2454, 2022.

[12] S. S. Das, S. Tiwari, V. Rangamgari, and S. C. Mondal, "Performance of iterative successive interference cancellation receiver for LDPC coded OTFS," in *2020 IEEE Int. Conf. on Advanced Netw. and Telecommun. Systems (ANTS), New Delhi, India*. IEEE, 2020, pp. 1–6.

[13] A. Thomas, N. Sangeeta, K. Deka, S. Sharma, and A. Rajesh, "OTSM-SCMA: Code-domain NOMA based orthogonal time sequency multiplexing modulation," in *2023 Nat. Conf. on Commun. (NCC), Guwahati, India*. IEEE, 2023, pp. 1–6.

[14] P. Raviteja, Y. Hong, E. Viterbo, and E. Biglieri, "Practical pulse-shaping waveforms for reduced-cyclic-prefix OTFS," *IEEE Trans. on Veh. Technol.*, vol. 68, no. 1, pp. 957–961, 2019.

[15] K. Deka, A. Thomas, and S. Sharma, "OTFS-SCMA: A code-domain NOMA approach for orthogonal time frequency space modulation," *IEEE Trans. on Commun.*, vol. 69, no. 8, pp. 5043–5058, 2021.

[16] A. Thomas, K. Deka, S. Sharma, and N. Rajamohan, "IRS-assisted OTFS system: Design and analysis," *IEEE Trans. on Veh. Technol.*, vol. 72, no. 3, pp. 3345–3358, 2022.

[17] G. D. Surabhi and A. Chockalingam, "Low-complexity linear equalization for OTFS modulation," *IEEE Commun. Lett.*, vol. 24, no. 2, pp. 330–334, 2020.

[18] H.-G. Ryu, J. S. Park, and J.-S. Park, "Threshold IBO of HPA in the predistorted OFDM communication system," *IEEE Trans. on Broadcast.*, vol. 50, no. 4, pp. 425–428, 2004.

[19] S. V. Zhidkov and R. Dinis, "Belief propagation receivers for near-optimal detection of nonlinearly distorted OFDM signals," in *2019 IEEE 89th Veh. Technol. Conf. (VTC2019-Spring), Kuala Lumpur, Malaysia*. IEEE, 2019, pp. 1–6.

[20] L. Smaini, *RF analog impairments modeling for communication systems simulation: application to OFDM-based transceivers*. John Wiley & Sons, 2012.

[21] K. Zhong, X. Lei, and S. Li, "Wiener filter preprocessing for OFDM systems in the presence of both nonstationary and stationary phase noises," *EURASIP J. on Advances in Signal Process.*, vol. 2013, pp. 1–9, 2013.

[22] A. Singh, S. Sharma, K. Deka, and V. Bhatia, "DL-based OTFS signal detection in presence of hardware impairments," *IEEE Wireless Commun. Lett.*, vol. 12, no. 9, pp. 1533–1537, 2023.